

On the self-consistent modeling of a traveling wave sustained nitrogen discharge

V. Guerra,^{a)} E. Tatarova, F. M. Dias, and C. M. Ferreira

Centro de Física dos Plasmas, Instituto Superior Técnico, 1049-001 Lisboa, Portugal

(Received 6 August 2001; accepted for publication 3 December 2001)

We present a self-consistent formulation to study low-pressure traveling wave (azimuthally symmetric surface transverse magnetic mode) driven discharges in nitrogen. The theoretical model is based on a self-consistent treatment of the electron and heavy particle kinetics, wave electrodynamics, gas thermal balance, and plasma-wall interactions. The solution provides the axial variation (as a result of nonlinear wave power dissipation along the wave path) of all discharge quantities and properties of interest, such as the electron energy distribution function and its moments, population densities of all relevant excited and charged species [$N_2(X^1\Sigma_g^+, \nu)$, $N_2(A^3\Sigma_u^+, a'^1\Sigma_u^-, B^3\Pi_g, C^3\Pi_u, a^1\Pi_g, w^1\Delta_u)$, N_2^+ , N_4^+ , e], gas temperature, degree of dissociation [$N(^4S)$]/ N , mean absorbed power per electron, and wave attenuation. A detailed analysis of the energy exchange channels among the degrees of freedom of the heavy particles is presented. Particular attention is paid to the axial variation of the gas and wall temperatures, which affect in a complex way the discharge operation. For the high electron densities and reduced electric fields achieved at 2.45 GHz, it is shown that the contribution of exothermic reactions involving excited molecules in metastable states to the total gas heating can be significant. The role of the triplet $N_2(A^3\Sigma_u^+)$ metastable state as an energy “reservoir” that pumps translational modes of gas particles is pointed out. A strong correlation between the degree of dissociation, the concentration of metastable $N_2(A^3\Sigma_u^+)$, $N(^2D, ^2P)$ particles, and surface kinetics is shown to exist. Spatially resolved measurements of the gas and wall temperatures, electron density, and wave propagation characteristics provide a validation of the model’s predictions. © 2002 American Institute of Physics. [DOI: 10.1063/1.1446229]

I. INTRODUCTION

Technological applications of molecular plasmas usually call for a detailed investigation of the transport and reactions of numerous neutral and charged species and of the energy exchange channels in the plasma source, in order to predict correctly the general trends of discharge behavior and the relevant species concentration. As far as microwave plasma generation is concerned, the investigation of discharges sustained by travelling surface waves (SWs) continues to provide major breakthroughs due to their flexible operation and their accessibility to a variety of diagnostics which, in combination with modeling, has had a pronounced impact on the understanding of hf discharges in general.¹⁻⁷ Considering the literature, one notes that long cylindrical plasma columns in inert gases have been intensively investigated both theoretically and experimentally since SW discharge’s inception. Self-consistent modeling of such systems has been extensively developed in the limit of the collisionless approach for wave electrodynamics, but usually neglecting the influence of the gas heating on the discharge physics.⁶⁻¹⁰ The operation of traveling wave sustained discharges in molecular gases, like nitrogen, is, however, far more complex due to the subtle and complex nonlinear coupling between plasma kinetics, wall conditions, and wave propagation. Although detailed models for dc discharges in nitrogen have been de-

veloped in the past,¹¹⁻¹⁶ the degree of sophistication of recent theoretical models for surface wave sustained discharges in nitrogen is less improved.¹⁷⁻¹⁹

This lesser degree of sophistication results, in part, from the nonequilibrium nature of low-pressure discharges, which requires simultaneous calculations of the strongly coupled electron and the heavy particles distributions, taking into account numerous particle interactions, both in the plasma bulk and at the wall, whose rate coefficients are unfortunately subject to large uncertainties. As is well known, the vibrational manifold of the electronic ground state in nitrogen discharges influences dramatically the whole discharge kinetics.¹¹⁻¹⁴ An additional problem is the intrinsic complexity of the self-consistent interdependence of the wave dynamics and the different balances governing the discharge production, which results in spatial nonuniformities. The nonlinear wave power dissipation along the discharge length induces axial variations of the discharge parameters, which are nonlinearly coupled to the absorbed power, and of the wall conditions (for example, the wall temperature). Spatially inhomogeneous gas heating leads to spatial variations in the gas temperature T_g , which affect in a complex way the discharge operating mechanisms.¹⁸⁻²⁰ A difficult and still poorly understood aspect of nitrogen discharges is the strong coupling between volume kinetics and interface (wall) conditions. Plasma-wall interactions, especially those involving dissociated nitrogen atoms and metastable species, play an

^{a)}Electronic mail: vguerra@theta.ist.utl.pt

important role in the whole discharge physics. Wall reactions determine the probabilities of reassociation of dissociated atoms and of destruction of metastable species, and thus they can affect the concentration of atoms and of other active species in the plasma bulk. It should be stressed that to date there is no satisfactory understanding of the nitrogen atom production and loss in relation to the discharge operation conditions.^{15,16,21–23} The dissociation kinetics has not previously been investigated consistently with the main discharge balances and wave propagation.

The major weakness of the existing theories of surface wave sustained discharges in molecular gases is their lack of completeness and self-consistency, since such important physical aspects as wave electrodynamics, gas heating, plasma–wall interactions, and atom kinetics are neglected in one way or another.^{18,24} A proper description can only be achieved by coupling the particle balance equations for all relevant charged and neutral species to the electron Boltzmann equation, the gas thermal balance, and the equations describing wave propagation and power dissipation. In this work we present a self-consistent approach of this type for a surface wave sustained nitrogen discharge. In particular, attention is paid to the energy exchange pathways between degrees of freedom of the heavy particles and the dissociation kinetics of nitrogen molecules. An experimental validation of the model predictions is also carried out as part of the present investigation.

The organization of the article is the following. In Sec. II the basic equations that self-consistently describe the axial structure of the discharge are presented and discussed. The numerical approach used to solve the set of equations is presented in Sec. III. An analysis of the discharge properties and their axial variations is given in Sec. IV. In particular, calculations of the electron energy distribution function (EEDF) and energy averaged quantities, and of the densities of all relevant species are presented as a function of the axial coordinate. Calculations of wave and discharge characteristics for different operating conditions are also provided. A detailed analysis of the various mechanisms of gas heating and atom kinetics is also carried out. It is shown that the main model predictions agree satisfactorily with experiments. Finally, Sec. V summarizes the principal conclusions of this investigation.

II. STATEMENT OF THE PROBLEM

In this section we discuss the self-consistent modeling of a microwave discharge sustained by a propagating azimuthally symmetric ($m=0$) surface wave at a frequency $f = \omega/2\pi$. The plasma column is generated in a cylindrical dielectric tube with permittivity ϵ_d . The z coordinate is directed along the tube axis and the wave propagates along this axis with wave vector $k = \alpha + i\beta$ (β and α are the axial wavenumber and the attenuation coefficient, respectively). As the wave propagates and creates its own propagating structure, the wave power flow decreases since the wave power is progressively absorbed by the plasma electrons. Subsequently, the electrons dissipate this power by collisions with the gas particles, i.e., the gas is excited, ionized, and

heated, and the energy is redistributed among translational (gas heating) and internal (i.e., vibrational, rotational, and electronic) modes. Gas and wall heating result in a change of the neutral density (under nearly isobaric conditions) and wall temperature along the tube. There is a self-consistent interplay between wave dynamics, properties of the generated plasma, and conditions at the interface (wall). To account for this, all the quantities concerning the generated plasma column, wall conditions, and wave propagation should be coupled self-consistently. Two important aspects of discharge physics are investigated self-consistently here, namely:

- (i) axial variation of different steady-state discharge balances: electron and heavy particle balance, electron energy balance, gas thermal balance, etc.;
- (ii) characteristics of the surface wave propagation along the generated inhomogeneous plasma column, i.e., axial variation of the wave dispersion characteristics and wave power balance.

For a self-consistent modeling, the input parameters of the theory are the usual externally controlled ones, namely, gas pressure, wave frequency, tube radius, and electron density at the position of the launcher (which is controlled through the power delivered to the launcher). In order to derive the axial variation of all quantities of interest, the model is based on a set of coupled equations for the plasma bulk describing the kinetics of free electrons, the vibrational kinetics of molecules in the electronic ground state, the kinetics of excited electronic states of molecules and atoms, the chemical kinetics of neutrals and ions, the gas thermal balance, and the charged particle balance determining the electric field sustaining the discharge. Further, a set of equations for the wave dispersion properties and power balance is incorporated in order to close the formulation.

A. Particle kinetics

1. Kinetics of free electrons

The EEDF is determined by solving the quasistationary homogeneous electron Boltzmann equation. Assuming the anisotropy caused by spatial inhomogeneities and the field to be sufficiently small, the electron velocity distribution is approximated by the usual two-term expansion in spherical harmonics. As shown experimentally,²⁵ for the pressures of interest here, the EEDF may be satisfactorily described in the local approach limit, i.e., the spatial diffusion of electrons is slower than their diffusion in energy space. Electron collisions of the first and the second kind and electron–electron collisions are accounted for. Since vibrationally excited molecules in nitrogen discharges constitute an appreciable fraction of the total molecular population, the EEDF is generally a function of the vibrational distribution function (VDF). The electron transport parameters and the rate coefficients calculated from the EEDF are functions of the reduced electric field E/N (N is the total density of the neutrals) and of the VDF. Although the SW electric field is radially inhomogeneous, the radial variation of the gas temperature, and correspondingly that of the neutral density, contribute to a flatten-

TABLE I. Inelastic and superelastic electron collisions.

Process	Reference
$e + N_2(X^1\Sigma_g^+, \nu=i) \rightarrow N_2(X^1\Sigma_g^+, \nu=j) + e$ with $i, j=0-8, i < j$	26
$e + N_2(X^1\Sigma_g^+, \nu=j) \rightarrow N_2(X^1\Sigma_g^+, \nu=i) + e$ with $i, j=0-8, i < j$	26
$e + N_2(X^1\Sigma_g^+, \nu=0) \rightarrow N_2(Y) + e$ for $Y=A^3\Sigma_u^+, B^3\Pi_g, C^3\Pi_u, B'^3\Sigma_u^-, W^3\Delta_u, E^3\Sigma_u^+$ $a'^1\Sigma_u^-, a^1\Pi_g, a''^1\Sigma_g^+, c'^1\Sigma_u^+, c^1\Pi_u, b^1\Pi_u, b'^1\Sigma_u^+, w^1\Delta_u$	26
$e + N_2(X^1\Sigma_g^+, \nu=0) \rightarrow N_2^+ + e + e$ (Z1)	27
$e + N_2(A^3\Sigma_u^+) \rightarrow N_2^+ + e + e$ (Z2)	28
$e + N_2(B^3\Pi_g) \rightarrow N_2^+ + e + e$ (Z3)	29
$e + N_2(a'^1\Sigma_u^-) \rightarrow N_2^+ + e + e$ (Z4)	29
$e + N_2(w^1\Delta_u) \rightarrow N_2^+ + e + e$ (Z5)	29
$e + N_2(a^1\Pi_g) \rightarrow N_2^+ + e + e$ (Z6)	29
$e + N_2(A^3\Sigma_u^+) \rightarrow e + N_2(B^3\Pi_g)$	29
$e + N_2(A^3\Sigma_u^+) \rightarrow e + N_2(X^1\Sigma_g^+)$	29
$e + N_2(A^3\Sigma_u^+) \rightarrow e + N_2(C^3\Pi_u)$	29
$e + N(^4S) \rightarrow e + N(^2D, ^2P)$	15

ing of the profile of the reduced electric field E/N . Since the EEDF is a function of E/N , the assumption of an essentially constant EEDF across the tube radius seems justified. The inelastic and superelastic processes taken into account and the sources used for the corresponding cross-section data are given in Table I.

Under steady-state conditions the power absorbed from the SW field per electron θ is equal to the net power lost per electron due to all kinds of electron collisions (leading to ionization, excitation, de-excitation, and dissociation of N_2 molecules). The corresponding electron power balance can be written as¹⁸

$$\theta(z) = -\frac{2}{3} \frac{e}{m_e} \int_0^\infty u^{3/2} \left[\frac{E(z)}{\sqrt{2}} \right] \frac{v_{em}(u)}{[v_{em}^2(u) + \omega^2]} \frac{\partial f_o}{\partial u} du$$

$$= \chi \langle u v_{em} \rangle + \sum_{i,j} u_{ij} \langle v_{ij} \rangle. \quad (1)$$

Here $f_o(u)$ is the isotropic part of the EEDF, v_{em} is the total momentum transfer collision frequency (collisions with N_2 and N), $\langle v_{ij} \rangle$ are the collision frequencies for electronic and vibrational excitation and de-excitation, and dissociation, i and j denoting the initial and final states, respectively; u_{ij} are the corresponding thresholds; $\chi = 2m_e/M$ (two times the electron–molecule mass ratio) is the energy transfer coefficient for elastic electron–molecule collisions.

The left-hand side of (1) represents the mean absorbed power per electron, i.e., $\theta(z)$ at a given position. The two terms on the right-hand side represent, respectively, the mean elastic energy loss rate and the net rate of energy loss in collisions with nitrogen molecules and atoms via the processes of vibrational and electronic excitation and de-excitation, N_2 dissociation, and atomic excitation. As a result of superelastic collisions, the electron Boltzmann equation and the local electron power balance equation should be coupled to the rate balance equations for electronically and vibrationally excited heavy species. However, only superelastic collisions with vibrationally excited molecules in the electronic ground state need to be considered, due to the high

population of these states. Further, due to the high degree of dissociation, a discharge in a mixture N_2-N must be considered.

2. Heavy particle kinetics

Due to the significant population in the vibrationally excited levels of the electronic ground state $N_2(X^1\Sigma_g^+, \nu)$ the Boltzmann equation is coupled to the system of rate balance equations for these populations through both inelastic and superelastic $e-V$ collisions. The various processes considered in the system of steady state equations for the populations $\delta_\nu = N_\nu/N$ in the levels $N_2(X^1\Sigma_g^+, \nu)$, with $0 \leq \nu \leq 45$, are listed in Table II. They account for $e-V$ collisions, electron dissociation ($e-D$), $V-V$ and $V-T$ energy exchanges (the latter including collisions with both N_2 and nitrogen atoms N), dissociation by $V-V$ and $V-T$ collisions ($V-D$), atomic reassociation (R), and deactivation of vibrationally excited molecules through collisions with the wall (W). We note that only single quantum transitions, which are the most likely ones, have been considered in the $V-V$ and $V-T$ collisional exchange processes. The sole exception concerns $V-T$ exchanges in N_2-N collisions, in which the effects of multi-quantum transitions are known to be important. The $V-D$ reactions take into account dissociation by $V-V$ and $V-T$ processes which are modeled as a transition from the last bound level $\nu=45$ to a pseudolevel in the continuum. The equations and mechanisms accounted for are described in detail in previous papers,^{11,12,15-18} to which the reader should refer for further information.

In addition to all electron and vibrational kinetic processes, the model includes the reactions determining the population densities of six excited molecular electronic states $N_2(A^3\Sigma_u^+, a'^1\Sigma_u^-, B^3\Pi_g, C^3\Pi_u, a^1\Pi_g, w^1\Delta_u)$. The radial profile of excited metastable particles is assumed to be a zero-order Bessel function. The rate equations are deduced by taking into account the collisional and the radiative processes given in Tables I and III, along with the corresponding data and pertinent references.

TABLE II. Kinetics of $N_2(X^1\Sigma_g^+)$ molecules.

$e-V$	$e+N_2(X^1\Sigma_g^+, \nu) \rightleftharpoons e+N_2(X^1\Sigma_g^+, w)$
$V-V$	$N_2(X^1\Sigma_g^+, \nu)+N_2(X^1\Sigma_g^+, w) \rightleftharpoons N_2(X^1\Sigma_g^+, \nu-1)+N_2(X^1\Sigma_g^+, w+1)$
$V-T$	$N_2(X^1\Sigma_g^+, \nu)+N_2 \rightleftharpoons N_2(X^1\Sigma_g^+, \nu-1)+N_2$
$V-T (N_2-N)$	$N_2(X^1\Sigma_g^+, \nu)+N \rightleftharpoons N_2(X^1\Sigma_g^+, w < \nu)+N$ $N_2(X^1\Sigma_g^+, \nu)+N \rightleftharpoons N+N_2(X^1\Sigma_g^+, w < \nu)$
W	$N_2(X^1\Sigma_g^+, \nu)+wall \rightarrow N_2(X^1\Sigma_g^+, \nu-1)$
$e-D$	$e+N_2(X^1\Sigma_g^+, \nu) \rightarrow e+N(^4S)+N(^4S)$ $e+N_2(X^1\Sigma_g^+, \nu) \rightarrow e+N(^4S)+N(^4D)$
$V-D$	$N_2(X^1\Sigma_g^+, \nu)+N_2(X^1\Sigma_g^+, \nu=45) \rightarrow N_2(X^1\Sigma_g^+, \nu-1)+N+N$
R	$N_2+N_2(X^1\Sigma_g^+, \nu=45) \rightarrow N_2+N+N$ $N+N \rightarrow N_2(X^1\Sigma_g^+, \nu=0)$

Following the analysis in Ref. 12 the excitation of electronic states by electron impact was treated as a single energy loss process assuming that all the molecules are in the ground vibrational level $N_2(X^1\Sigma_g^+, \nu=0)$. It was further assumed that all processes leading to the formation of a ground electronic state molecule populate the level $\nu=0$ only.

In the present model two types of positive ions, N_2^+ and N_4^+ have been considered. The N_2^+ ions are created by electron impact ionization of neutral molecules, stepwise ionization (Table I) and associative ionization (Table IV), while N_4^+ ions are created mainly by associative ionization processes involving $N_2(A^3\Sigma_u^+)$ and $N_2(a'^1\Sigma_u^-)$ metastable states. We assume the same branching ratio for the production of N_2^+ and N_4^+ by associative ionization. Additional channels contributing to the creation or the destruction of positive ions are also listed in Table IV. The main processes of removal of charged particles are ambipolar diffusion to the wall and bulk dissociative recombination (Table V). Electron rate coefficients for dissociative recombination of ions have been calculated using semi-empirical formulas reported in Ref. 31 as a function of the electron kinetic temperature.

3. Charged particle balance and maintaining field

The maintenance electric field is self-consistently determined by solving the continuity equations for electrons and positive ions N_2^+ and N_4^+ together with the quasineutrality

condition $n_e = [N_2^+] + [N_4^+]$. The balance between the rates of charged particle production and loss determines the maintenance field self-consistently. In fact, the field strength necessary for the steady-state operation of the discharge is obtained from the balance between the total rate of ionization, including direct, associative [involving collisions between the metastable species $N_2(A^3\Sigma_u^+)$ and $N_2(a'^1\Sigma_u^-)$] and step-wise ionization [from $N_2(A^3\Sigma_u^+)$, $N_2(a'^1\Sigma_u^-)$, $N_2(w^1\Delta_u)$, $N_2(B^3\Pi_g)$ and $N_2(a^1\Pi_g)$] processes and the total rate of electronic losses due to diffusion to the wall, in the presence of N_2^+ and N_4^+ ions,¹⁷ and electron-ion bulk recombination. Taking into account the ionization and recombination processes listed in Tables I, III, IV, and V along with the corresponding rate coefficients, electrons satisfy the following continuity equation:

$$n_e N Z_1 + n_e N(A) Z_2 + n_e N(B) Z_3 + n_e N(a') Z_4 + n_e N(w^1) Z_5 + n_e N(a^1) Z_6 + N(a') N(A) k_{as1} + N(a')^2 k_{sa2} = n_e \frac{D_{ae}}{\Lambda_{eff}^2} + \alpha_{r1} n_e N_1 + \alpha_{r2} n_e N_2, \quad (2)$$

where A , a' , w^1 , B , and a^1 denote the states $N_2(A^3\Sigma_u^+)$, $N_2(a'^1\Sigma_u^-)$, $N_2(w^1\Delta_u)$, $N_2(B^3\Pi_g)$ and $N_2(a^1\Pi_g)$ respectively, D_{ae} is ambipolar diffusion coefficient for electrons in the presence of two types of positive ions, Λ_{eff} is an effective diffusion length which is determined assuming that both

TABLE III. Collisional-radiative processes involving electronically excited molecules.

Process	k (m^3s^{-1})	References
$N_2(a'^1\Sigma_u^-)+N_2(X) \rightarrow N_2(B^3\Pi_g)+N_2(X)$	1.9×10^{-19}	30, 31
$N_2(a^1\Pi_g)+N_2(X) \rightarrow N_2(a'^1\Sigma_u^-)+N_2(X)$	2.0×10^{-17}	32
$N_2(a^1\Pi_g) \rightarrow N_2(a'^1\Sigma_u^-) + hf$	$1.91 \times 10^2 s^{-1}$	33
$N_2(C^3\Pi_u) \rightarrow N_2(B^3\Pi_g) + hf$	$27.4 \times 10^6 s^{-1}$	34
$N_2(B^3\Pi_g) \rightarrow N_2(A^3\Sigma_u^+) + hf$	$2 \times 10^5 s^{-1}$	35
$N_2(a^1\Pi_g) \rightarrow N_2(X, \nu=0) + hf$	$1.8 \times 10^4 s^{-1}$	32
$N_2(A^3\Sigma_u^+)+N_2(A^3\Sigma_u^+) \rightarrow N_2(B^3\Pi_g)+N_2(X, \nu=0)$	7.7×10^{-17}	36
$N_2(A^3\Sigma_u^+)+N_2(A^3\Sigma_u^+) \rightarrow N_2(C^3\Pi_u)+N_2(X, \nu=0)$	1.5×10^{-16}	37
$N_2(B^3\Pi_g)+N_2 \rightarrow N_2(A^3\Sigma_u^+)+N_2$	$0.95 \times 3.0 \times 10^{-17}$	37
$N_2(B^3\Pi_g)+N_2 \rightarrow N_2(X, \nu=0)+N_2$	$0.05 \times 3.0 \times 10^{-17}$	38
$N_2(B'^3\Sigma_u^-) \rightarrow N_2(B^3\Pi_g) + hf$		16
$N_2(w^1\Delta_u) \rightarrow N_2(a^1\Pi_g) + hf$	$6.5 \times 10^2 s^{-1}$	39
$N_2(A^3\Sigma_u^+) + N(^4S) \rightarrow N_2(X, \nu=6-9) + N(^2P)$	4×10^{-17}	40
$N_2(A^3\Sigma_u^+) + N_2(X, \nu=5-15) \rightarrow N_2(B^3\Pi_g) + N_2(X, \nu=0)$	2×10^{-17}	37

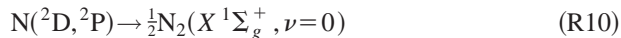
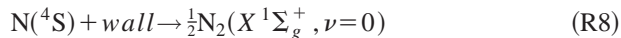
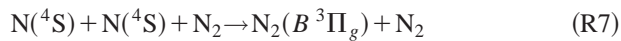
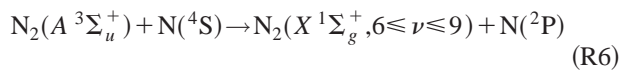
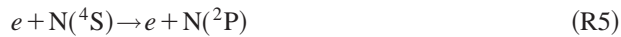
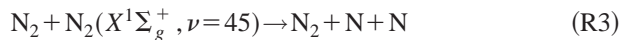
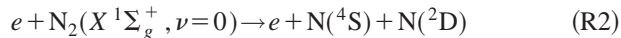
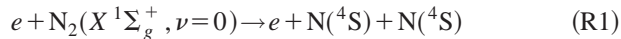
TABLE IV. Rate constants for reactions involving positive ions.

Reactions	Rate constant (m^3s^{-1})	Reference
$\text{N}_2(A^3\Sigma_u^+) + \text{N}_2(a' ^1\Sigma_u^-)$	$K_{\text{as1}} = 1.0 \times 10^{-17}$	16
$\left\{ \begin{array}{l} \text{N}_2^+ + \text{N}_2 + e \\ \text{N}_4^+ + e \end{array} \right.$		
$\text{N}_2(a' ^1\Sigma_u^-) + \text{N}_2(a' ^1\Sigma_u^-)$	$K_{\text{as2}} = 5.0 \times 10^{-17}$	16
$\left\{ \begin{array}{l} \text{N}_2^+ + \text{N}_2 + e \\ \text{N}_4^+ + e \end{array} \right.$		
$\text{N}_4^+ + \text{N}_2 \rightarrow \text{N}_2^+ + 2\text{N}_2$	$2.1 \times 10^{-22} \exp(Tg/121)$	41
Three-body collisions		
$\text{N}_2^+ + \text{N}_2 + \text{N}_2 \rightarrow \text{N}_4^+ + \text{N}_2$	$6.8 \times 10^{-29} (300/Tg)^{1.64} \text{ m}^6/\text{s}$	42

types of ions reach the corresponding ion sound speed at the plasma-sheath boundary,¹⁷ and N_1 and N_2 stand for the N_2^+ and N_4^+ ion density, respectively.

4. Dissociation kinetics

The dissociation kinetics is an important issue due to the numerous volume and wall processes involving atoms which influence strongly discharge operation. The kinetics of nitrogen atoms in the ground [$\text{N}(^4\text{S})$] and metastable [$\text{N}(^2\text{D}, ^2\text{P})$] states is taken into account by considering the following reactions (some of the reactions are listed in Tables I and III and rewritten here):¹⁶



The main source of ground state $\text{N}(^4\text{S})$ nitrogen atoms for the conditions considered is electron impact dissociation (R1, R2). One of the loss channels of $\text{N}(^4\text{S})$ is reassociation on the wall (R8). According to the work of Guerra and Loureiro,¹⁶ the probability $\zeta = 5 \times 10^{-4}$ has been assumed for this process. The metastable atoms $\text{N}(^2\text{D}, ^2\text{P})$ are created by electron impact (R4, R5) or through the important quenching reaction of $\text{N}_2(A^3\Sigma_u^+)$ in collisions with $\text{N}(^4\text{S})$ atoms (R6). It is assumed that most of the metastable atoms

TABLE V. Rate constants for dissociative recombination of ions.^a

Reactions	Rate constant (m^3s^{-1})
$e + \text{N}_2^+ \rightarrow \text{N} + \text{N}$	$\alpha_{r1} = 4.8 \times 10^{-13} (300/T_e)^{1/2}$
$e + \text{N}_4^+ \rightarrow \text{N}_2 + \text{N}_2$	$\alpha_{r2} = 2.0 \times 10^{-12} (300/T_e)^{1/2}$

^aSee Ref. 31.

are converted into the ground state $\text{N}(^4\text{S})$ through collisions with the wall and quenching in collisions with heavy particles, which is symbolically expressed by (R9). A total effective probability $\gamma = 0.8-0.9$ is used to describe these mechanisms. As shown in Ref. 16, γ is in fact close to one, i.e., most excited metastable atoms are converted to the ground state. The remaining fraction of excited atoms $\text{N}(^2\text{D}, ^2\text{P})$, corresponding to the probability $\gamma_r = 1 - \gamma$, is assumed to reassociate into $\text{N}_2(X^1\Sigma_g^+, \nu=0)$ (R10).

B. Gas heating

In order to account for gas and wall heating, the gas thermal balance equation must be incorporated in the system of equations. In the present 1D formulation, under nearly isobaric conditions, neglecting axial transport and assuming heat conduction is the predominant cooling mechanism, the stationary gas thermal balance equation can be expressed in the form:¹⁹

$$\frac{8\lambda(T_g)}{R^2} (T_g - T_w) = Q_{\text{in}}. \quad (3)$$

Here, T_g is the radially averaged gas temperature, T_w is the wall temperature, and $\lambda(T_g)$ is the thermal conductivity.⁴³ Q_{in} accounts for the total net power transferred per unit volume into the translation mode from volume and wall sources of heat. A parabolic radial profile of the gas temperature has been assumed. The wall temperature is introduced as an input parameter as experimentally obtained (see below). The calculations of the total gas heating term (Q_{in} in Eq. 3) take into account all collisional processes that convert some energy into the gas translational mode, namely:

- (i) $V-V$ vibrational relaxation mechanisms of N_2 molecules in N_2-N_2 collisions.

$$Q_{\text{in}}^{(V-V)} = \sum_{\nu=1}^{45} [\text{N}_2(X, \nu)] \sum_{w=1}^{45} [\text{N}_2(X, w-1)] \times P_{\nu, \nu-1}^{w-1, w} \Delta E_{\nu, \nu-1}^{w-1, w},$$

- (ii) $V-T$ relaxation mechanisms of N_2 molecules in N_2-N_2 collisions.

$$Q_{\text{in}}^{(V-T)} = [\text{N}_2] \sum_{\nu=1}^{45} \{ [\text{N}_2(X, \nu)] P_{\nu, \nu-1} - [\text{N}_2(X, \nu-1)] P_{\nu-1, \nu} \} \Delta E_{\nu, \nu-1},$$

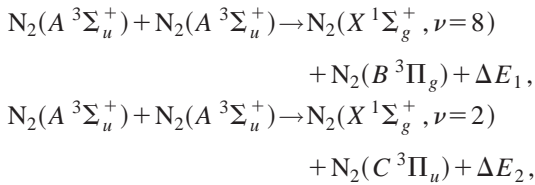
- (iii) $V-T$ relaxation mechanisms of N_2 molecules in N_2-N collisions.

$$Q_{in}^{N_2-N} = [N] \sum_{\nu=1}^{45} [N_2(X, \nu)] \sum_{w=1}^{45} P_{\nu,w}^{N_2-N} \Delta E_{\nu,w},$$

- (iv) vibrational deactivation at the wall

$$Q_{in}^{wall} = \sum_{\nu=1}^{45} [N_2(X, \nu)] \nu_w \Delta E_{\nu, \nu-1} \xi,$$

- (v) pooling reactions^{20,44}



$$\Delta E_1 = 2 \text{ eV}; \quad \Delta E_2 = 0.4 \text{ eV},$$

- (vi) deactivation of metastable states on the wall

$$Q_{in}^Y = [N_2(Y)] \frac{D}{\Lambda^2} \Delta E_Y \xi,$$

$$Y = N_2(A^3\Sigma_u^+), N_2(a'^1\Sigma_u^-), N_2(a^1\Pi_g), N_2(w^1\Delta_u),$$

- (vii) elastic collisions of electrons with neutrals

$$Q_{in}^{el} = n_e [N_2] P_{el}.$$

Here, $P_{\nu, \nu-1}^{w-1, w}$, $P_{\nu, \nu-1}$, $P_{\nu, w}^{N_2-N}$ are the rate coefficients for the corresponding processes; ΔE_Y is the energy of the excited state; ν_w is the frequency of wall losses;¹⁶ $\Lambda = a/2.4$; P_{el} is the average energy transferred from electrons to neutrals in elastic collisions; ξ is the accommodation coefficient, which determines the part of the energy returned to the gas phase that dissipates into heat due to deactivation of metastable or vibrationally excited species on the wall. It should be noted that in process (v) it is assumed that half of the available energy goes into gas heating.^{20,44}

C. Wave-to-plasma power coupling

The self-consistent interplay between wave electrodynamics and discharge balances results in inhomogeneous power dissipation along the wave path, consequently in an axial variation of the discharge parameters. These parameters are nonlinearly coupled to the absorbed power. The theoretical treatment of the wave-to-plasma coupling in the model is based on a simultaneous solution of the wave and the electron power balance equations.¹⁸ The mechanism of power transfer can be expressed quantitatively by introducing θ —the mean power needed to maintain an electron-ion pair. The absorbed power in a plasma slice of thickness Δz at position z is $\Delta P = \theta(z) S n_e(z) \Delta z$, S denoting the plasma cross section. Under steady state conditions, the spatial rate of wave power change dP/dz is equal to the power absorbed by the electrons per unit discharge length. The local power balance equation is therefore

$$\theta(z) S n_e(z) = - \frac{dP}{dz} = 2\alpha(z) P(z_0) \times \exp\left(- \int_{z_0}^z 2\alpha(x) dx\right). \quad (4)$$

This equation linking the wave power flux to the power absorbed by the electrons in the discharge provides the axial description of the discharge structure. By differentiating Eq. (4), the following equation is readily obtained for the axial gradient of the electron density:

$$\frac{dn_e}{dz} = - \frac{2\alpha n_e}{1 - \frac{n_e}{\alpha} \frac{d\alpha}{dn_e} + \frac{n_e}{\theta} \frac{d\theta}{dn_e}}. \quad (5)$$

As usual, the attenuation coefficient α is derived by solving the local wave dispersion equation.^{45,46} As far as wave propagation is concerned, the plasma response can be described by the frequency dependent dielectric permittivity ϵ_{pl} :

$$\epsilon_{pl}(z) = 1 - \frac{\omega_{pl}^2(z)}{\omega(\omega + i\nu_{eff})}$$

where $\omega_{pl}(z) = (n_{eff}(z)e^2/m_e\epsilon_o)^{1/2}$ (e and m_e are the electron charge and mass, respectively, and ϵ_o is the vacuum dielectric permittivity) and n_{eff} and ν_{eff} are ω -dependent effective values of the electron density and electron-neutral collision frequency. As pointed out in Ref. 7, considering these effective parameters is essential since the electron-neutral collision frequency for momentum transfer $\nu_{em}(u)$ in nitrogen is strongly energy dependent. Under the assumption of a slow variation of the plasma permittivity along the wave path, “local” field equations with a “local” dispersion equation are used to obtain the spatial rate of wave power losses. The coupling structure generates an azimuthally symmetric TM mode and the wave field components in cylindrical geometry are E_z , E_r and H_ϕ . The expressions for the fields are well known and can be found elsewhere.¹⁸ The wave dispersion characteristics can be obtained as usual by considering the continuity of the field tangential components across the interfaces. This provides the local dispersion equation (LDE) which can symbolically be expressed as:^{45,46}

$$D[\omega/\omega_{pl}(z), \omega a/c, \nu_{eff}(z)/\omega, \epsilon_d, k] = 0. \quad (6)$$

According to the experimental situation, solutions for constant ω and variable $\nu_{eff}(z)/\omega$ and $n_{eff}(z)$ along the wave path are searched for.

III. METHOD OF SOLUTION

A flow chart of the model and solution algorithm used is depicted in Fig. 1. The input parameters of the model are the wave frequency $\omega/2\pi$, tube radii a and b (inner and outer, respectively), pressure p , electron density at the position of the SW launcher $n_e(z_0)$ and the axial profile of the wall temperature $T_w(z)$.

The procedure starts with arbitrary values of the electric field E , vibrational (T_ν^o) and gas (T_g^o) temperatures. The electron Boltzmann equation is solved by iterations. In the calculations of the EEDF, the accuracy achieved in the electron power balance equation (1) (yielding the value of θ) is better than 10^{-5} . By using the rate coefficients for electron impact processes, the nonlinear set of equations for heavy particles and ions is solved by applying the Newton-Raphson method. The electric field is varied to satisfy the

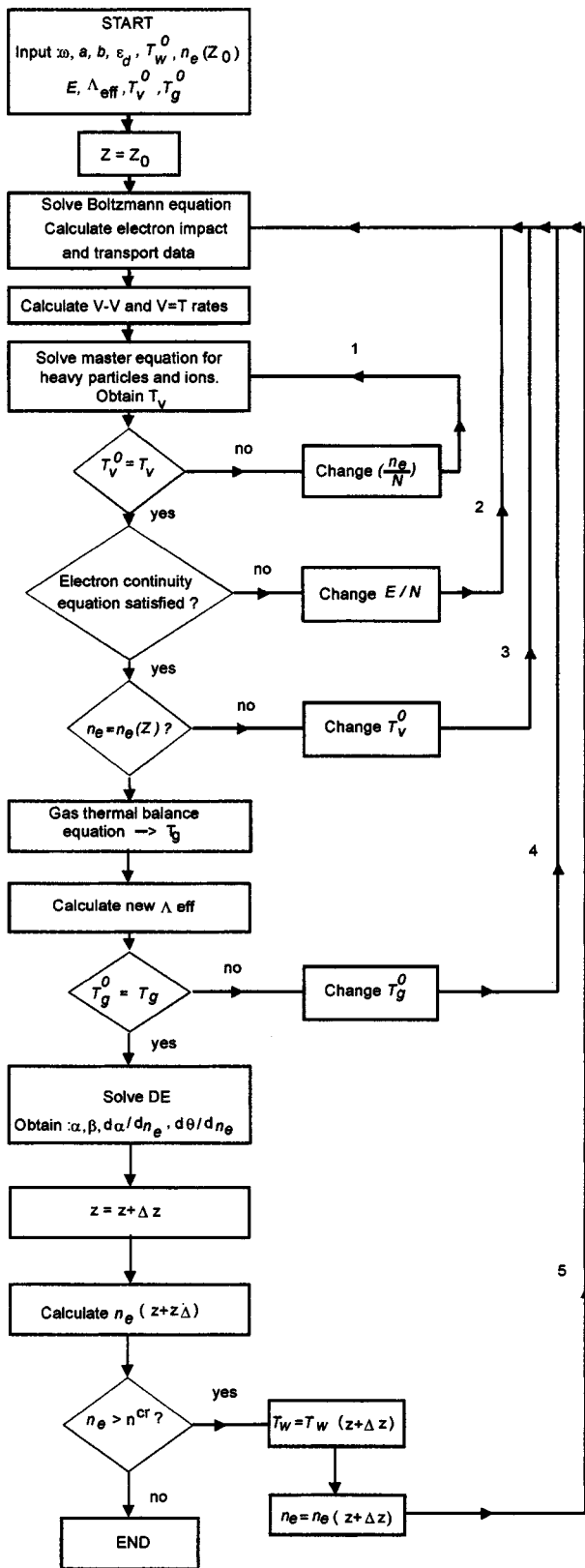


FIG. 1. Flow chart of the model.

electron continuity equation (2). For the electric field (E) determination, an accuracy better than 10^{-5} is achieved. As a result of the first (1), second (2), and third (3) iterative loops convergent solutions for the vibrational temperature T_v and the electric field maintaining the discharge is achieved for a

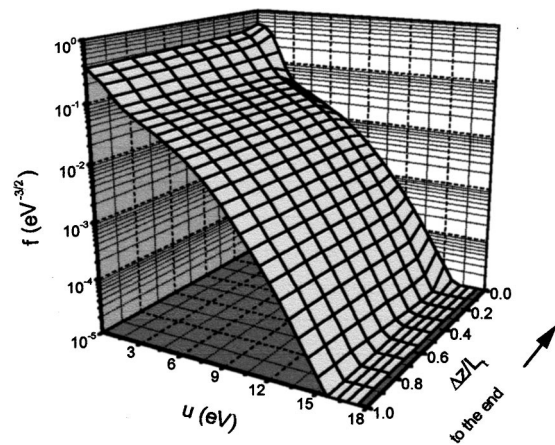


FIG. 2. Axial variations of the calculated EEDFs ($\omega/2\pi=500$ MHz, $p=0.5$ Torr).

given value of the electron density $n_e(z)$. Then, the gas thermal balance equation (3) is solved and a new iteration procedure (loop 4) determines a self-consistent value of T_g . Using the self-consistently calculated values of $n_{\text{eff}}(z)$ and $v_{\text{eff}}(z)$, the LDE is solved in complex algebra. The integration of Eq. (5) yields the new value of the electron density at the position $z + \Delta z$. Then the entire loop (5) is repeated for the next axial position. So, point by point, the discharge and the wave characteristics are calculated along the plasma column until n_e reaches the critical value $n_e^{\text{cr}} = [(n_e e^2 / m_e \epsilon_0)^{1/2}]$, where it is assumed the discharge stops.

The calculated results include the axial variation of the EEDF and its integrals, $\theta(z)$, $n_e(z)$, the VDF of the electronic ground state δ_v , the population densities of the electronically excited states N_2 ($A^3\Sigma_u^+, a'^1\Sigma_u^-, B^3\Pi_g, C^3\Pi_u, a^1\Pi_g, w^1\Delta_u$) and nitrogen atoms in ground state $N(^4S)$, electric field E , gas temperature T_g , and wave attenuation coefficient α .

IV. RESULTS AND DISCUSSION

This section presents an application of the model to two different cases of SW discharge operation. Experimental results that aim at checking some basic physical trends predicted by the model have been obtained in microwave discharges operating at the frequencies $\omega/2\pi=500$ MHz ($a=2.25$ cm, $b=2.5$ cm, $p=0.5$ Torr) and $\omega/2\pi=2.45$ GHz ($a=0.75$ cm, $b=0.9$ cm, $p=0.6$ Torr).

Considering the discharge at 500 MHz, Fig. 2 shows the variation of the EEDF along the discharge length. In order to unify all the results, the distance toward the end Δz is normalized to the total discharge length L_t . As noted, the electron-molecule energy exchange processes significantly influence the EEDF shape. The observed decrease in the energy interval 1.5–3 eV, as is well known, reflects the rapid rise of the vibrational cross sections in this energy range.^{11,12} This effect of “vibrational barrier” is well-pronounced close to the end ($\Delta z/L_t \rightarrow 0$), but is partly attenuated by superelastic collisions toward the SW launcher ($\Delta z/L_t \rightarrow 1$) due to the higher degrees of ionization, and thus higher vibrational excitation¹⁷ in this region. The degree of ionization, for the conditions considered, varies from approximately 10^{-5}

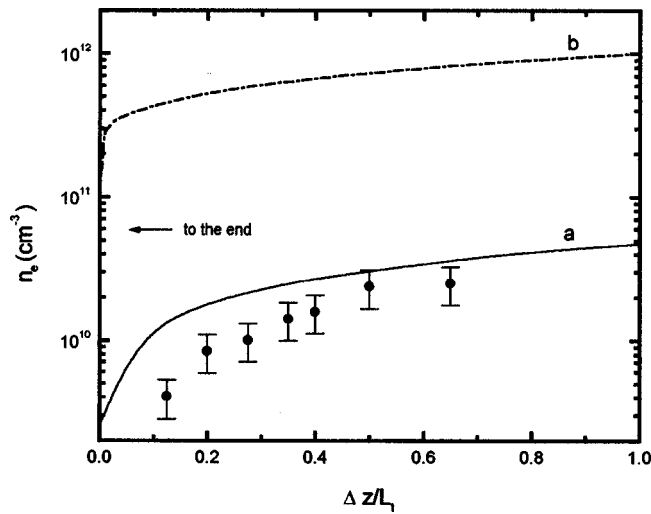


FIG. 3. Axial variation of the electron density (curves: calculations; •: experiment) (a) $\omega/2\pi=500$ MHz, $p=0.5$ Torr; (b) $\omega/2\pi=2.45$ GHz, $p=0.6$ Torr).

($\Delta z/L_t \rightarrow 1$) to about 10^{-6} close to the plasma column end ($\Delta z/L_t \rightarrow 0$) (see Fig. 3). The predicted values of $n_e(z)$ compare satisfactorily with experimental results obtained by a probe diagnostic technique¹⁷ as shown in Fig. 3.

The axial variation of the VDF of the electronic ground state $N_2(X^1\Sigma_g^+, \nu)$ is depicted in Figs. 4(a and b). Different regimes of population and depopulation of the vibrational levels can be identified from the shape of the VDFs. The VDF shape results as usual from the combined effects of e - V and V - V exchanges at low vibrational levels, of near resonant V - V exchanges at intermediate levels, which tend to form a plateau in this region, and to the simultaneous effects of vibrational dissociation and V - T exchanges at the highest levels.^{11,12,15,16} As can be seen from Fig. 4(a) for a low degree of ionization, the regions corresponding to the above mentioned mechanisms can be clearly identified. A small increase in the population of the high vibrational levels ($\nu > 35$) toward the column end should be noted.

At higher degrees of ionization (10^{-4} – 10^{-5}) [Fig. 4(b)], the calculated VDFs are considerably “excited” and exhibit significant changes along the discharge length. In order to characterize the degree of vibrational excitation, the vibrational temperature T_ν , defined as the characteristic vibrational temperature of a Treanor-like distribution that best fits the calculated fractional populations for $0 \leq \nu \leq 3$, is introduced.^{11,12} The corresponding axial variations of T_ν are shown in Fig. 4(c). The higher degrees of ionization and reduced fields achieved in the discharge at 2.45 GHz cause higher vibrational excitation of the lower vibrational levels i.e., higher vibrational temperatures. Further, as compared to the case of lower degrees of ionization [Fig. 4(a)], a considerable reduction of the plateau region occurs as shown in Fig. 4(b). The effect is more pronounced close to the SW launcher ($\Delta z/L_t \rightarrow 1$) due to the higher degrees of ionization and higher T_g .

The significant increase in the population density of the highest vibrational levels ($\nu > 30$) [Fig. 4(b)] toward the plasma column end ($\Delta z/L_t \rightarrow 0$) is a consequence of the high

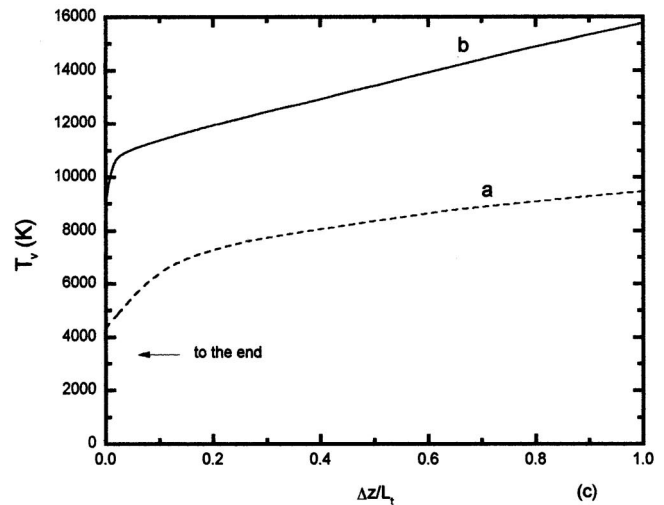
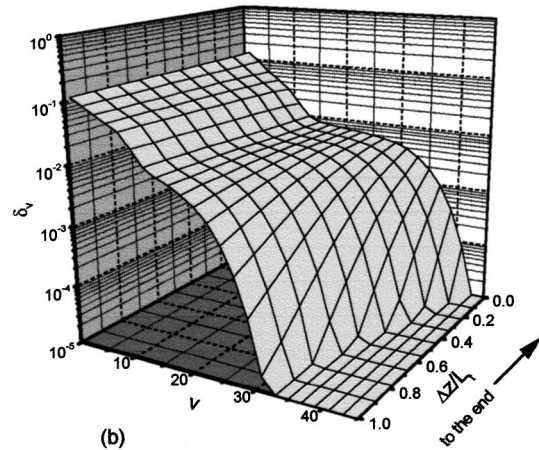
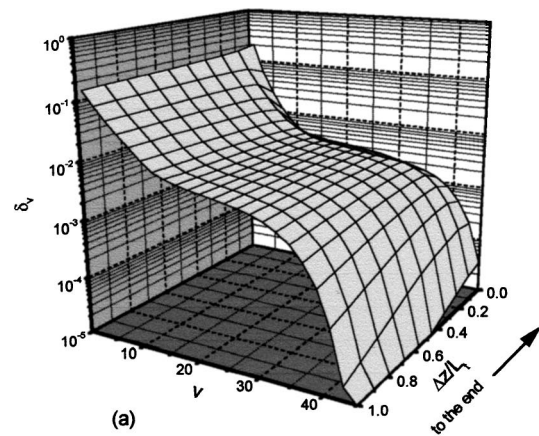
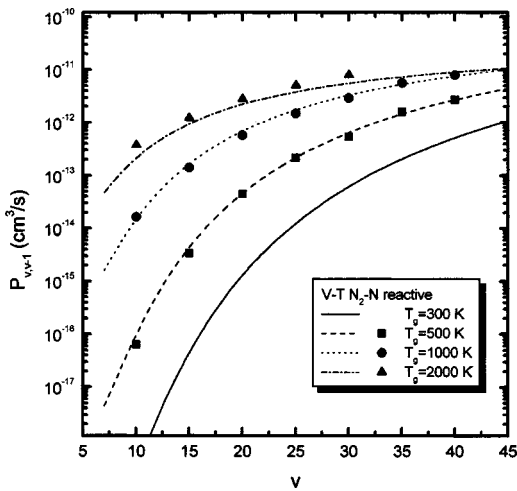


FIG. 4. Axial variation of the calculated VDFs (a) $\omega/2\pi=500$ MHz, $p=0.5$ Torr; (b) $\omega/2\pi=2.45$ GHz, $p=0.6$ Torr; (c) axial variation of the vibrational temperature.

V - T depopulation rates of the VDF by N_2 - N collisions. To understand this, one should note that the V - T rates for N_2 - N collisions increase with the ν -th quantum number by several orders of magnitude at constant gas temperature T_g and increase also as T_g increases,⁴⁷ as shown in Fig. 5. For higher vibrational levels, the V - T relaxation processes in N_2 - N collisions cause therefore a rapid falloff of the VDF. The obtained results clearly demonstrate that the simultaneous effects of the decrease in degree of ionization (n_e/N) and gas

FIG. 5. Rate coefficients for $V-T$ exchanges in N_2-N collisions (Ref. 47).

temperature (see below), cause a decrease in the population of the lower vibrational levels, (i.e., T_v) toward the end. At the same time, the decrease of the nitrogen atom density (see below) and T_g toward the end causes an increased population of the higher vibrational levels ($\nu > 30$) close to the discharge end ($\Delta z/L_t \rightarrow 0$) as a result of the decreasing influence of $V-T$ depopulation mechanisms in N_2-N collisions.

Calculated and measured axial distributions of the gas temperature are shown in Figs. 6 and 7. Also shown on these figures for completeness is the axial distribution of the measured wall temperature. An infrared sensitive nonperturbative measurement, using an electro-optical thermometer, provides experimental results for the axial variation of the wall temperature during the discharge operation. Note that the wall is cooled by natural convection only. The experimental gas temperatures were determined, as usual for nitrogen, by measuring the rotational distribution of the second positive system of nitrogen $N_2(C^3\Pi_u, \nu') \rightarrow N_2(B^3\Pi_g, \nu'')$ in the 375.5–379 nm wavelength range (i.e., 0–0 vibrational transition) assuming that the rotational and translational modes are in equilibrium.¹⁸ As observed, the gas temperature decreases nonlinearly from the position of the SW launcher toward the plasma column end as a consequence of the non-uniform wave power absorption along the wave path (see Fig. 8). The larger wave power absorption at 2.45 GHz results in a higher gas and wall temperatures. The experimental results clearly demonstrate that, to a first approximation, the gas temperature at a given axial position is a function of the power absorbed per unit length by the plasma electrons at that position.

At lower degrees of ionization [Fig. 6(a)], a good agreement between measured and calculated values of T_g is obtained. It is usually considered that gas heating in nitrogen discharges comes mainly from the $V-V$ and $V-T$ relaxation processes of the vibrationally excited N_2 molecules.⁴⁸ This is confirmed by the results presented in Fig. 6(b), where the relative contribution of the different gas heating channels along the discharge length is depicted. The excitation of vibrational levels by electron impact followed by $V-T$ relaxation in N_2-N multiquantum processes is the dominant gas

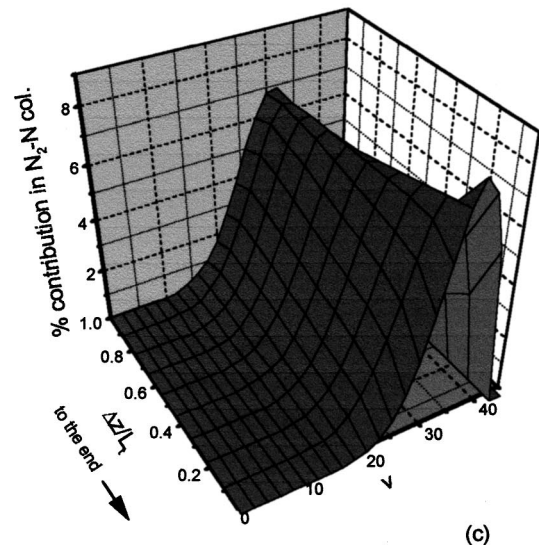
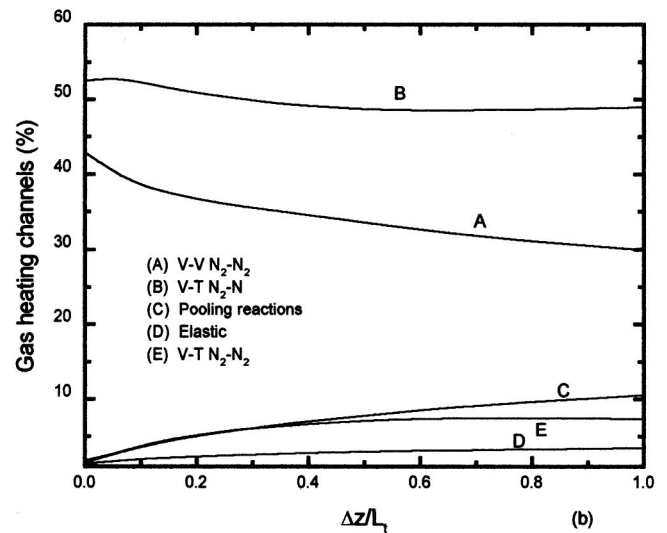
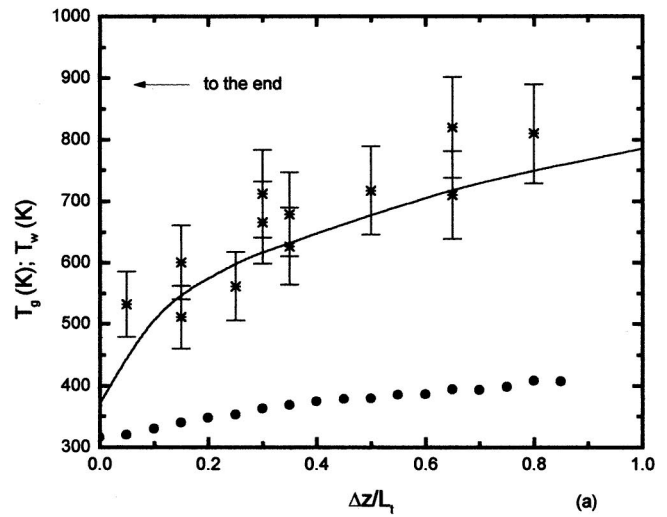


FIG. 6. (a) Axial variations of the gas (*) and wall (•) temperatures ($\omega/2\pi=500$ MHz, $p=0.5$ Torr); (b) Relative contribution of the different heating channels to the total gas heating; (c) Relative contribution of the vibrational levels of the electronic ground state to the channel associated with $V-T$ relaxation processes in N_2-N collisions.

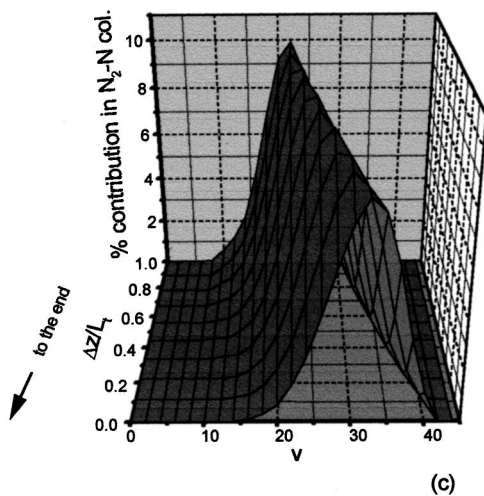
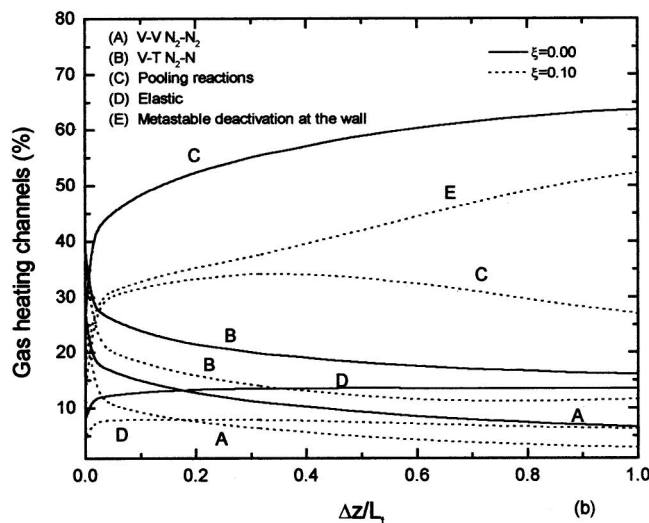
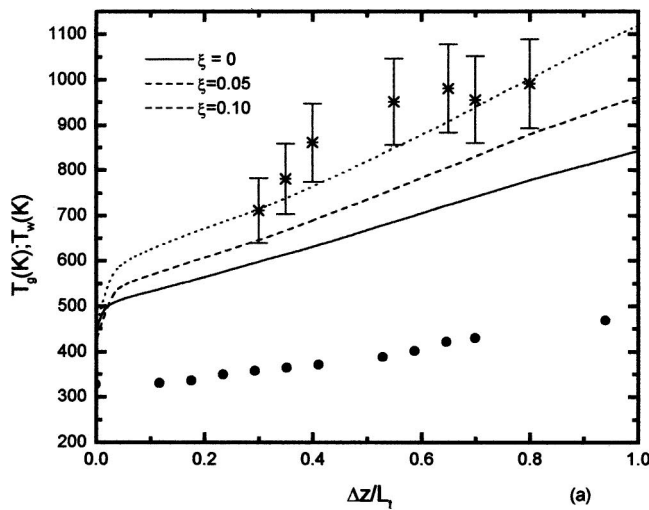


FIG. 7. (a) Axial variations of the gas (*) and wall (•) temperatures ($\omega/2\pi=2.45$ GHz, $p=0.6$ Torr); (b) Relative contribution of the different heating channels to the total gas heating; (c) Relative contribution of the vibrational levels of the electronic ground state to the channel associated with $V-T$ relaxation processes in N_2-N collisions.

heating mechanism for the conditions considered. This result is a consequence of the high $V-T$ depopulation rates of the VDF by N_2-N collisions. These effects are extremely important, even for the relatively small atomic concentrations of

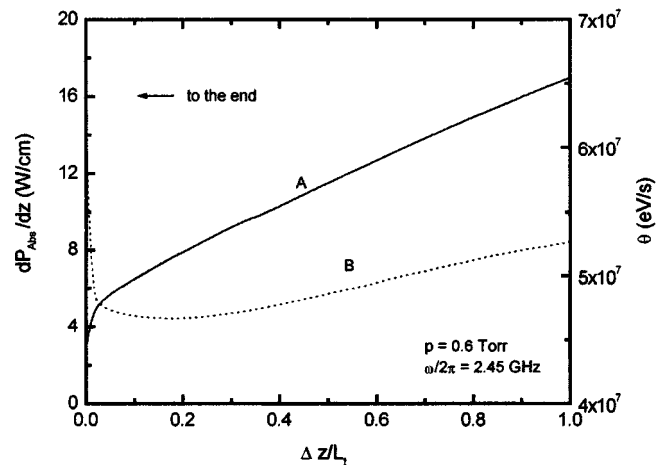
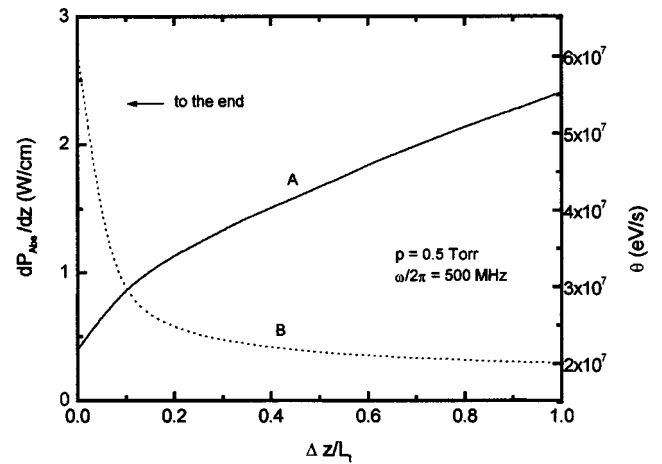


FIG. 8. Axial distribution of dP/dz (A) and θ (B).

about 10^{-2} obtained for these conditions (see below). It should be noted that including the contribution of the exothermic reactions at the wall, i.e., wall deactivation of the molecules in metastable states [channel (vi)], just results in slightly higher gas temperatures at the beginning of the discharge ($\Delta z/L_t \rightarrow 1$) where the population of these species is higher.

It is also instructive to analyze the relative contribution of the different vibrational levels to the main heating channel, i.e., $V-T$ relaxation in N_2-N collisions. This contribution is presented in Fig. 6(c). The correlation between the increased population in higher vibrational levels ($v = 25-35$) close to the end ($\Delta z/L_t \rightarrow 0$) [Fig. 4(a)], and the increase in their relative contribution to gas heating should be emphasized.

A different situation occurs at higher degrees of ionization, reduced effective electric fields, and molecular dissociation degrees (see below). Taking into account only the heating mechanisms associated with vibrationally excited molecules [processes (i), (ii), (iii), and (iv)] and the contribution of exothermic pooling reactions between $N_2(A^3\Sigma_u^+)$ metastable species [channel (v)] results in significantly lower (about twice) T_g values than experimentally obtained [Fig.

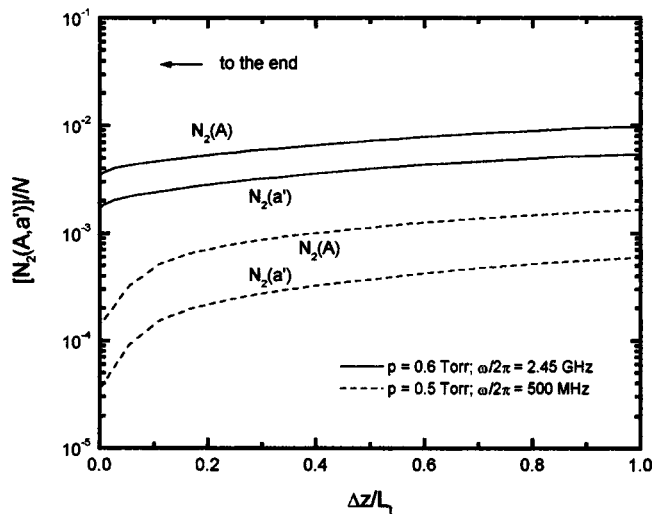


FIG. 9. Axial distribution of $N_2(A^3\Sigma_u^+)$ and $N_2(a'^1\Sigma_u^-)$ metastable particles.

7(a)]. Additional sources must therefore contribute to the total gas heating in this case. Plausible sources can be exothermic reactions at the wall involving long-lived species, such as N_2 metastable molecules [channel (vi)], or channel (v). Due to the high degrees of ionization and reduced effective electric fields, high populations of N_2 molecules in metastable states can be reached (see Fig. 9 below). The metastable molecules $N_2(A^3\Sigma_u^+)$, $N_2(a'^1\Sigma_u^-)$, $N_2(a^1\Pi_g)$, and $N_2(w^1\Delta_u)$ are lost due to the diffusion to the wall. Therefore, wall deactivation of metastables may contribute to the gas heating mechanism even if, for instance, only 10% of the available energy returns to the gas phase and dissipates into heat as the calculations show [Fig. 7(a)]. However, the possible contribution of other heating mechanisms should be also kept in mind.

The competitive interplay of the different gas heating mechanisms along the discharge length, depicted in Fig. 7(b), demonstrates that the channel involving metastable particles can play an important role in gas heating for high degrees of ionization and reduced fields of the order of 10^{-4} and 17×10^{-15} (V/cm²), respectively. As a consequence of the decreasing density of the metastables close to the end, the contribution of the processes involving metastable species decreases. At the same time the relative contribution of the V - T relaxation processes in N_2 - N collisions sharply increases as $(\Delta z/L_t \rightarrow 0)$. As can be seen from Fig. 7(c), this fact is strongly correlated with the increase in population in the higher vibrational levels of the electronic ground state $N_2(X^1\Sigma_g^+, \nu)$ [Fig. 4(b)] and the increased relative contribution of these levels to heating by V - T processes in N_2 - N collisions.

The above analysis is only intended to show that exothermic processes involving long-lived metastable species can contribute significantly to total gas heating and provide a better explanation of the measured gas temperature profiles. However, due to the existing uncertainties in collisional data, particularly those concerning plasma-wall interactions, no quantitative conclusion can yet be drawn about the predominant heating mechanisms.

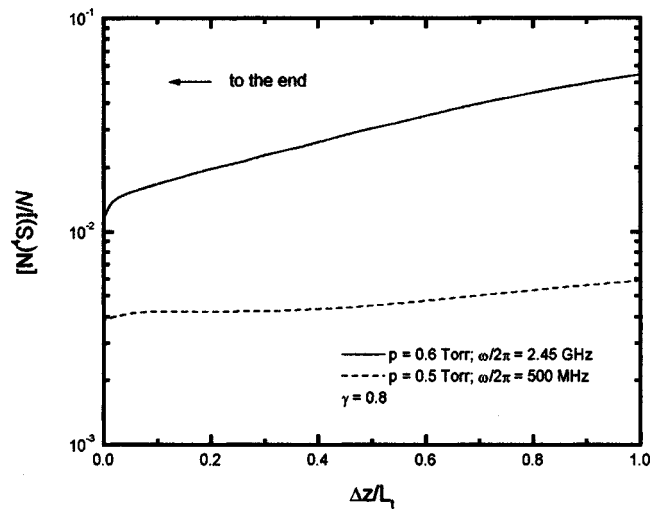


FIG. 10. Axial distribution of the relative number density $[N(^4S)]/N$ of nitrogen atoms.

The variation of θ , self-consistently calculated on the basis of the electron energy balance (Eq. 1), is plotted in Fig. 8 (dotted lines). As seen, θ follows a different behavior than dP_{abs}/dz (Eq. 4). Due to the sharp decrease of the electron density (see Fig. 3), θ exhibits a sharp increase close to the plasma column end ($\Delta z/L_t \rightarrow 0$).

An important problem in N_2 discharges is the kinetics of nitrogen atoms $N(^4S)$. At the pressures of interest here, the main source channel for N atoms is electron impact dissociation (reactions R1, R2) and one of the main loss channels is $N(^4S)$ re-association at the wall (R8), with probability ζ . As previously discussed, we assume that most excited atoms $N(^2D, ^2P)$ are converted into the ground state $N(^4S)$ through collisions at the wall and quenching with a total effective probability $\gamma=0.8$ – 0.9 . Due to the lack of data and for the sake of simplicity, a constant (i.e., temperature independent) probability for atomic re-association ($\zeta=5 \times 10^{-4}$) at the wall has been assumed. Thus, as a first approximation it is assumed that the axial variation of ζ does not significantly

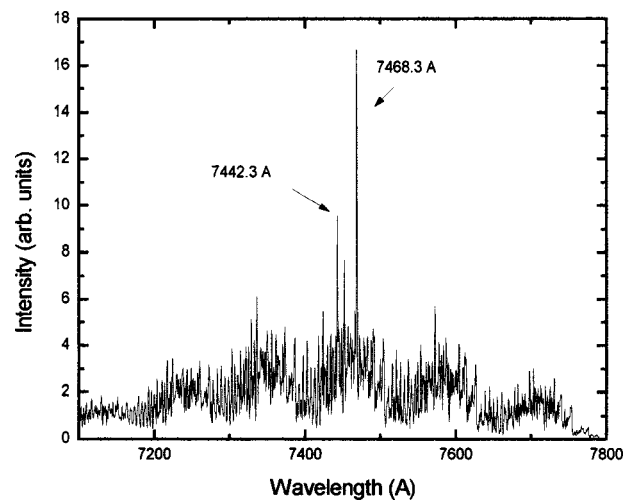


FIG. 11. Emission spectrum of the discharge operating at 2.45 GHz ($p = 0.6$ Torr).

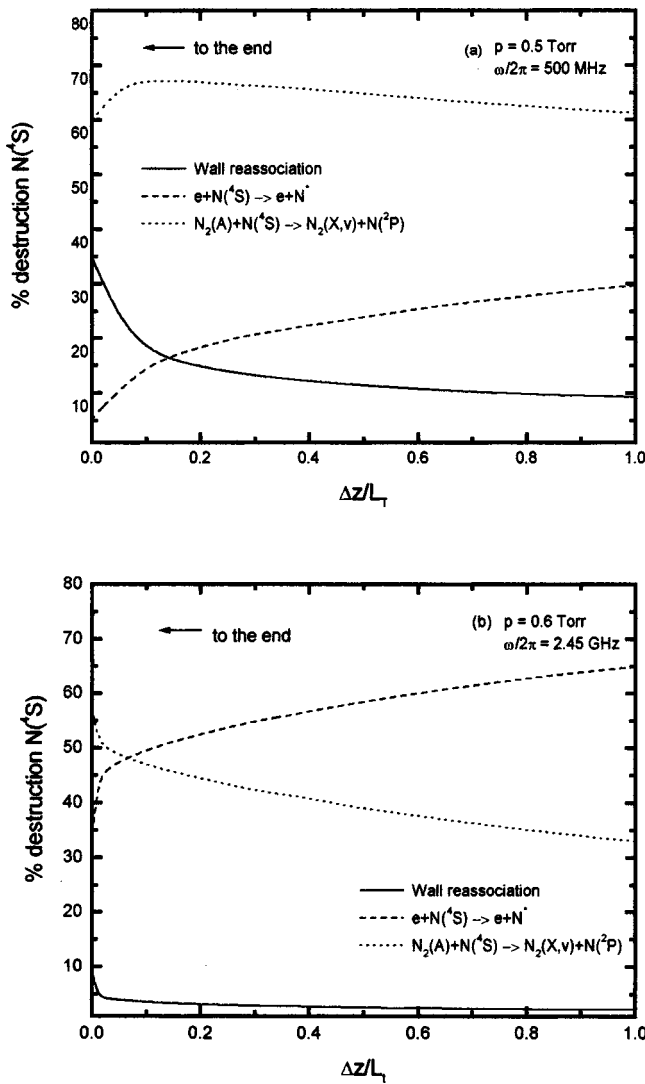


FIG. 12. Percentage contribution of the various loss channels of $N(^4S)$ atoms.

affect the N atom axial profile. It should be noted that including axial variations of ζ (as a result of T_w axial variation) would require detailed consideration of N atom surface kinetics, which is beyond present knowledge.

As expected, the higher electron densities and reduced fields for the discharge operating at 2.45 GHz lead to higher dissociation degrees than in the case of the discharge at 500 MHz, as shown in Fig. 10. This result is confirmed by intense atomic lines (belonging to the $3p\ ^4S^0 \rightarrow 3s\ ^4P$ transition) detected in the emission spectrum of the discharge at 2.45 GHz (see Fig. 11), but which are not easily detected in the 500 MHz discharge. As far as the main production mechanism of N atoms is electron impact dissociation, the decrease of n_e and E/N along the discharge results in a decrease of the N atom number density. If there were no correlations with the populations of excited nitrogen atoms $N(^2D, ^2P)$, metastables and the wall-temperature-dependent surface kinetics, the atomic concentration would be nearly proportional to the electron density. However, the variation of the relative density of N atoms is less than one order of magnitude along the whole discharge length, which indicates

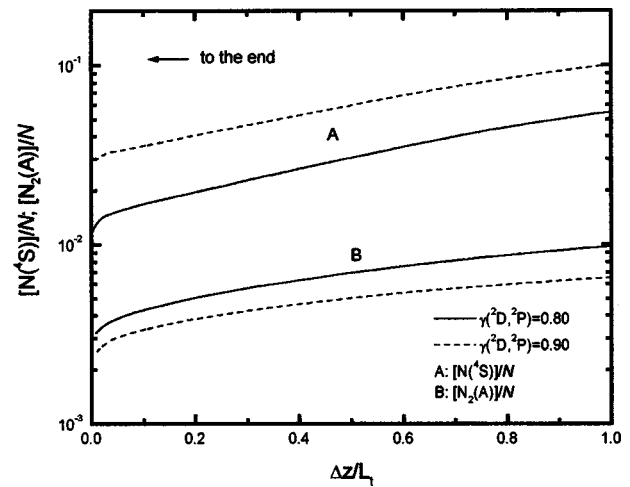
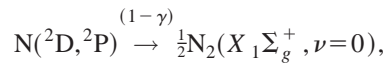
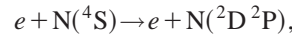


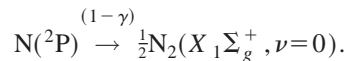
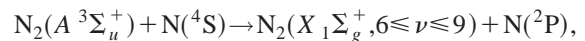
FIG. 13. Correlation of nitrogen atoms relative density with $N_2(A\ ^3\Sigma_u^+)$ density.

that the nitrogen atom density does not simply follow n_e as can be seen from Figs. 3 and 10.

Figure 12 shows the percentage contribution of the following loss processes of $N(^4S)$ atoms: wall reassociation (R8), effective destruction by electron impact as a result of the two-step reaction



and effective quenching by the metastable $N_2(A\ ^3\Sigma_u^+)$ by the two-step reaction



The competition between these channels results in different predominant loss mechanisms at low and high degrees of dissociation and ionization as shown in Figs. 12(a) and 12(b), respectively. Quenching of $N_2(A\ ^3\Sigma_u^+)$ by $N(^4S)$ atoms is the dominant loss channel at low ionization degrees [Fig. 12(a)]. At higher electron densities, electron impact destruction dominates. It should be stressed, however, that the present results are to be regarded as merely indicative due to the large uncertainties in input data. Particularly, this concerns the values of the probabilities for wall reassociation of ground state atoms and wall destruction of metastable atoms.

The strong sensitivity to plasma-wall interactions, and the coupling existing between the population densities of $N(^4S)$ and $N_2(A\ ^3\Sigma_u^+)$ is demonstrated in Fig. 13. Changing the probability γ for wall deactivation of $N(^2D, ^2P)$ from 0.9 to 0.8 results in a decrease in the $N(^4S)$ number density by a factor of two and a corresponding increase in the $N_2(A\ ^3\Sigma_u^+)$ population density by a similar factor. The results obtained clearly show that an accurate determination of the $N(^4S)$ atom density is inevitably coupled to an accurate treatment of the kinetics of plasma-wall interactions in correlation with the gas thermal balance (i.e., T_g) and the wave electro-

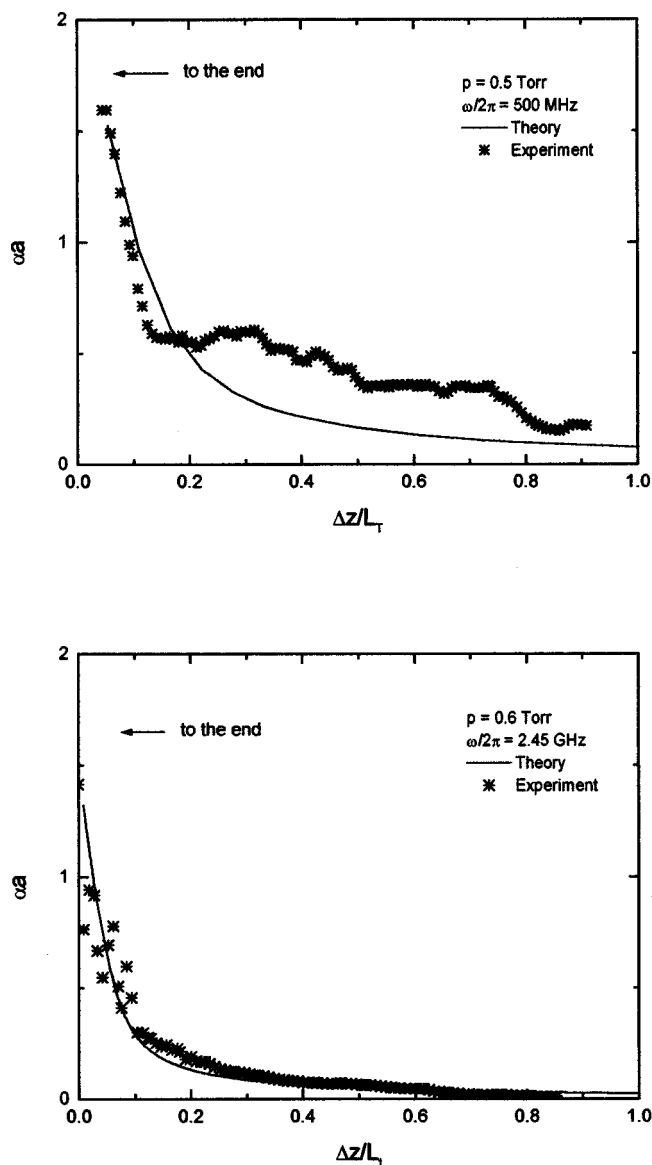


FIG. 14. Axial variation of the wave attenuation coefficient α .

dynamics. Future work should concentrate on this point in order to get deeper insight into the discharge physics.

In order to test the spatial rate of wave power losses predicted by the model, the wave attenuation coefficient has been measured. The SW electric field outside the plasma column allows one to detect the radial electric field or the associated power by using an antenna aligned normally to the tube wall and movable in the axial direction. Power sensitive recording along the wave path provides measurements of $P(z)$ and of the local values of the spatial rate of wave power loss, i.e., $\alpha(z) = -\frac{1}{2}[1/P(z)][dP(z)/dz]$.

Theoretical and experimental values of $\alpha(z)$ shown in Fig. 14 are seen to be in good agreement. The gradual increase of $\alpha(z)$ along the major part of the column is followed by a sharp rise close to the end. This is a consequence of the simultaneous decrease in electron density and increase of ν_{eff} towards the discharge end (note that under nearly isobaric conditions, since T_g decreases along the discharge (Figs. 6(a) and 7(a), the neutral density increases as $\Delta z/L_t$

$\rightarrow 0$). We can conclude that the electrodynamic description of the model accounts well for the wave power absorption along its path.

VI. CONCLUSION

In the present work, a self-consistent numerical model for a microwave nitrogen discharge sustained by a traveling surface wave has been developed and applied to investigate the discharge structure under different operation conditions. The model is based on the solution of a coupled system of equations including the electron Boltzmann equation, particle balance equations for all relevant charged and neutral species, the gas thermal balance equation, and the equations describing wave propagation and power dissipation. The solution provides the axial distribution of all discharge quantities and properties of interest such as the EEDF and its moments, excited and charged species population densities [$N_2(X^1\Sigma_g^+, \nu)$, $N_2(A^3\Sigma_u^+, a'^1\Sigma_u^-, B^3\Pi_g, C^3\Pi_u, a^1\Pi_g, w^1\Delta_u)$, N_2^+, N_4^+], gas temperature, degree of dissociation [$N(^4S)$]/ N , mean absorbed power per electron θ , wave attenuation α , etc.

Due to the inhomogeneous wave power absorption along the wave path, the main discharge parameters, nonlinearly coupled to that power, also present axial variations. A detailed analysis of the energy exchange pathways among translational (gas heating) and internal (vibrational, electronic) modes of the heavy particles is presented. To achieve an accurate description of the discharge kinetics, the axial distribution of gas temperature T_g must be taken into consideration, because the variation of T_g results in changes in the neutral density and some rate coefficients have a strong temperature dependence (for instance, those for V - T energy exchanges). It is usually considered that gas heating in nitrogen discharges is determined by V - V and V - T energy exchanges between vibrationally excited molecules and molecules and atoms. This is confirmed by experimental and theoretical results for SW discharge operation at 500 MHz. For these conditions of low degrees of ionization (10^{-5} – 10^{-6}), the excitation of vibrational levels by electron impact followed by V - T and V - V relaxation in N_2 - N and N_2 - N_2 collisional processes is in fact the dominant gas heating mechanism. However, for a SW discharge operating at 2.45 GHz, higher degrees of ionization and reduced effective electric fields are obtained, which results in higher populations of nitrogen molecules in electronically excited metastable states. Consequently, gas heating channels involving these states can play an important role in the total gas heating. The triplet $N_2(A^3\Sigma_u^+)$ metastable state plays the role of an energy “reservoir” for translational modes of gas particles. It was further shown that the simultaneous $N(^4S)$ atom density decrease and the increase in the population density of the higher vibrational levels $N_2(X^1\Sigma_g^+, \nu=20-35)$ toward the plasma column end cause an increase in the relative contribution of high vibrational levels ($\nu=20-35$) to heating by V - T multiquantum energy exchanges in N_2 - N collisions.

The creation of ground state atoms $N(^4S)$ is mainly due to electron impact dissociation, and the contribution of vibrational dissociation is negligible, contrary to what has been considered in many recent works. This is because the effec-

tive depopulation of the higher vibrational levels of the electronic ground state by V - T energy exchanges in N_2 - N collisions causes a strong decrease in the vibrational dissociation contribution. The loss channels for ground state atoms are atomic reassociation at the wall, electron impact excitation and quenching of $N_2(A^3\Sigma_u^+)$ in collisions with $N(^4S)$ atoms. At different frequency of discharge operation, different loss mechanisms of ground $N(^4S)$ state atoms are predominant. The results demonstrate a crucial influence of the $N(^2D,^2P)$ metastable kinetics on the $N(^4S)$ density. Small variations in the deactivation probability γ for $N(^2D,^2P)$ atoms result in significant changes in the $N(^4S)$ density. The strong coupling existing between the $N_2(A^3\Sigma_u^+)$ and $N(^4S)$ population densities should also be pointed out.

In conclusion, a deeper physical understanding of nitrogen discharges sustained by a traveling surface wave requires further theoretical and experimental investigation. The results clearly show that an accurate determination of the $N(^4S)$ density in traveling wave driven discharge requires a reliable treatment of the kinetics of plasma-wall interactions, including surface and bulk $N(^2D,^2P)$ metastable atoms kinetics in correlation with the main discharge balances. Work in this direction is in progress and will be reported in the future.

- ¹C. M. Ferreira, F. M. Dias, and E. Tatarova, in *Advances Technologies Based on Wave and Beam Generated Plasmas*, edited by H. Schluter and A. Shivarova (Kluwer Academic Dordrecht, 1999) p. 311.
- ²H. Sugai, I. Ghanashev, and M. Nagatsu, *Plasma Sources Sci. Technol.* **7**, 192 (1998).
- ³I. Ghanashev, H. Sugai, *Phys. Plasmas* **7**, 3051 (2000).
- ⁴I. Ghanashev, M. Nagatsu, S. Morita, and H. Sugai, *J. Vac. Sci. Technol. A* **16**, 1537 (1999).
- ⁵I. Ghanashev, M. Nagatsu and H. Sugai, *Jpn. J. Appl. Phys.* **36**, 337 (1997).
- ⁶A. B. Sá, C. M. Ferreira, S. Pasquiers, C. Boisse-Laporte, P. Leprince, and J. Marec, *J. Appl. Phys.* **70**, 4147 (1991).
- ⁷C. M. Ferreira, in *Nonequilibrium Processes in Partially Ionized Gases*, edited by M. Capitelli and J. N. Bardsley (Plenum, New York, 1990) pp. 187–212.
- ⁸U. Kortshagen, *Phys. Rev. E* **49**, 4369 (1994).
- ⁹U. Kortshagen and H. Schluter, *J. Phys. D* **25**, 1574 (1992).
- ¹⁰U. Kortshagen, *J. Phys. D* **26**, 1230 (1993).
- ¹¹J. Loureiro and C. M. Ferreira, *J. Phys. D* **22**, 67 (1989).
- ¹²C. M. Ferreira and J. Loureiro, *J. Phys. D* **22**, 76 (1989).
- ¹³M. Cacciatore, M. Capitelli, and C. Gorse, *Chem. Phys.* **66**, 141 (1982).
- ¹⁴C. Gorse, M. Cacciatore, M. Capitelli, S. De Benedictis, and G. Dilecce, *Chem. Phys.* **119**, 63 (1988).
- ¹⁵V. Guerra and J. Loureiro, *J. Phys. D* **28**, 1903 (1995).
- ¹⁶V. Guerra and J. Loureiro, *Plasma Sources Sci. Technol.* **6**, 361 (1997).
- ¹⁷E. Tatarova, F. M. Dias, C. M. Ferreira, V. Guerra, J. Loureiro, E. Stoykova, I. Ghanashev, and I. Zhelyazkov, *J. Phys. D* **30**, 2663 (1997).
- ¹⁸E. Tatarova, F. M. Dias, C. M. Ferreira, and A. Ricard, *J. Appl. Phys.* **85**, 49 (1999).
- ¹⁹V. Guerra, E. Tatarova, F. M. Dias, A. Ricard and C. M. Ferreira, in *Proceedings of the 14th International Symposium on Plasma Chemistry*, Prague, Czech Republic (Institute of Plasma Physics ASCR), p. 687.
- ²⁰V. Guerra, P. Sa, and J. Loureiro, *J. Phys. D* **34**, 1745 (2001).
- ²¹C. Boisse-Laporte, C. Chave-Normand and J. Marec, *Plasma Sources Sci. Technol.* **6**, 70 (1997).
- ²²D. Blois, P. Supiot, M. Barj, A. Chapput, C. Foissac, O. Dessaux, and P. Goudmand, *J. Phys. D* **31**, 2521 (1998).
- ²³P. Merel, M. Tabbal, M. Chaker, M. Moisan, and A. Ricard, *Plasma Sources Sci. Technol.* **7**, 550 (1997).
- ²⁴M. J. Pinheiro, G. Gousset, A. Granier, and C. M. Ferreira, *Plasma Sources Sci. Technol.* **7**, 524 (1998).
- ²⁵F. M. Dias, E. Tatarova, and C. M. Ferreira, *J. Appl. Phys.* **83**, 4602 (1998).
- ²⁶J. Loureiro and C. M. Ferreira, *J. Phys. D* **19**, 17 (1986).
- ²⁷D. Rapp and P. Englander-Golden, *J. Chem. Phys.* **43**, 1464 (1965).
- ²⁸R. S. Freund, R. C. Wetzel, and R. J. Shul, *Phys. Rev. A* **41**, 5861 (1990).
- ²⁹J. Bacri and A. Medani, *Physica B & C* **112**, 101 (1982).
- ³⁰L. G. Piper, *J. Chem. Phys.* **87**, 1625 (1987).
- ³¹A. I. Kossyi, A. Yu. Kostinsky, A. A. Matveyev, and V. D. Silakov, *Plasma Sources Sci. Technol.* **1**, 207 (1992).
- ³²W. J. Marinelli, W. J. Kessler, B. D. Green, and W. A. M. Blumberg, *J. Chem. Phys.* **90**, 2167 (1989).
- ³³N. S. Freund, *J. Chem. Phys.* **56**, 4344 (1972).
- ³⁴A. Lofthus and P. H. Krupenie, *J. Phys. Chem. Ref. Data* **6**, 113 (1977).
- ³⁵L. G. Piper, *J. Chem. Phys.* **91**, 864 (1989).
- ³⁶L. G. Piper, *J. Chem. Phys.* **88**, 6911 (1988).
- ³⁷L. G. Piper, *J. Chem. Phys.* **88**, 231 (1988).
- ³⁸L. G. Piper, *J. Chem. Phys.* **97**, 270 (1992).
- ³⁹M. E. Fraser, W. T. Rawlins and S. M. Miller, *J. Chem. Phys.* **88**, 538 (1988).
- ⁴⁰L. G. Piper, *J. Chem. Phys.* **90**, 7087 (1989).
- ⁴¹D. I. Slovetskii, *Mechanisms of Chemical Reactions in a Non-Equilibrium Plasma* (Nauka, Moscow, 1980).
- ⁴²H. Bohringer and F. Arnold, *J. Chem. Phys.* **77**, 5534 (1982).
- ⁴³J. O. Hirschfelder, C. F. Curtiss, and R. B. Bird, *Molecular Theory of Gases and Liquids* (Wiley, New York, 1964).
- ⁴⁴J. P. Boeuf and E. E. Kunhardt, *J. Appl. Phys.* **60**, 915 (1986).
- ⁴⁵I. Ghanashev, I. Arestova, E. Tatarova, I. Zhelyazkov, and S. Stoykov, *J. Plasma Phys.* **58**, 633 (1997).
- ⁴⁶F. M. Dias, E. Tatarova, J. Henriques, and C. M. Ferreira, *J. Appl. Phys.* **85**, 2528 (1999).
- ⁴⁷A. Lagana, G. Ochoa de Asporu and E. Garcia, *Quasiclassical and quantum rate coefficients for the N_2 - N reaction*, Report from Università degli Studi di Perugia, 1996, (unpublished).
- ⁴⁸A. Garscadden and R. Nagpal, *Plasma Sources Sci. Technol.* **4**, 268 (1995).